Science Bulletin 67 (2022) 1702–1711

Contents lists available at ScienceDirect

Science Bulletin

journal homepage: www.elsevier.com/locate/scib

Article

Varying contributions of fast and slow responses cause asymmetric tropical rainfall change between CO_2 ramp-up and ramp-down

Shijie Zhou [a], Ping Huang [a,b,*], Shang-Ping Xie [c], Gang Huang [b,d,e], Lin Wang [a,b]

[a] Center for Monsoon System Research, Institute of Atmospheric Physics, Chinese Academy of Sciences, Beijing 100190, China
[b] State Key Laboratory of Numerical Modeling for Atmospheric Sciences and Geophysical Fluid Dynamics, Institute of Atmospheric Physics, Chinese Academy of Sciences, Beijing 100029, China
[c] Scripps Institution of Oceanography, University of California San Diego, La Jolla CA 92093, USA
[d] Laboratory for Regional Oceanography and Numerical Modeling, Pilot National Laboratory for Marine Science and Technology, Qingdao 266237, China
[e] College of Earth and Planetary Sciences, University of Chinese Academy of Sciences, Beijing 100049, China

ARTICLE INFO

Article history:
Received 7 February 2022
Received in revised form 6 May 2022
Accepted 7 May 2022
Available online 4 July 2022

Keywords:
Tropical rainfall
Fast and slow responses
Sea surface warming pattern
CDRMIP

ABSTRACT

Tropical rainfall is important for regional climate around the globe. In a warming climate forced by rising CO_2, the tropical rainfall will increase over the equatorial Pacific where sea surface warming is locally enhanced. Here, we analyze an idealized CO_2 removal experiment from the Carbon Dioxide Removal Model Intercomparison Project (CDRMIP) and show that the tropical rainfall change features a stronger pattern during CO_2 ramp-down than ramp-up, even under the same global mean temperature increase, such as the 2 °C goal of the Paris Agreement. The tropical rainfall during CO_2 ramp-down increases over the equatorial Pacific with a southward extension, and decreases over the Pacific intertropical convergence zone and South Pacific convergence zone. The asymmetric rainfall changes between CO_2 ramp-down and ramp-up result from time-varying contributions of the fast and slow oceanic responses to CO_2 forcing, defined as the responses to abrupt CO_2 forcing in the first 10 years and thereafter, respectively, in the abrupt-4xCO2 experiment. The fast response follows the CO_2 evolution, but the slow response does not peak until 60 years after the CO_2 peak. The slow response features a stronger El Niño-like pattern, as the ocean dynamical thermostat effect is suppressed under stronger subsurface warming. The delayed and stronger slow response leads to stronger tropical rainfall changes during CO_2 ramp-down. Our results indicate that returning the global mean temperature increase to below a certain goal, such as 2 °C, by removing CO_2, may fail to restore tropical convection distribution, with potentially devastating effects on climate worldwide.

1. Introduction

Anthropogenic changes in tropical rainfall are of great importance to regional climate via atmospheric teleconnections [1,2] and by affecting the El Niño–Southern Oscillation [3]. In a warming climate, global precipitation is projected to increase under energetic constraint [1,4]. The mechanisms for tropical rainfall changes under increasing CO_2 radiative forcing have been widely studied, including the wet-get-wetter [4,5] and warmer-get-wetter [6–10] mechanisms. The former highlights the increased rainfall in convective regions, and the latter focuses on the influence of the sea surface temperature (SST) warming pattern.

Towards the goal of returning the global mean temperature increase to below a certain goal, the CO_2 concentration could need to ramp down after the current ramp up (hereafter referred to simply as CO_2 ramp-up/ramp-down) [11,12]. One of the most important climate changes during CO_2 ramp-down is the stronger hydrological cycle than during ramp-up at the same CO_2 level [13–16], due to the previously accumulated heat in the ocean. Recent studies have revealed asymmetrical responses of the intertropical convergence zone and East Asian summer rainfall [17,18], highlighting the implications of an idealized CO_2 removal scenario to the real world. Tropical rainfall change is likely to differ between the ramp-up and ramp-down periods, but the details of this asymmetry are not well understood. The pattern of tropical rainfall change can be influenced by processes at multiple timescales, such as the fast direct radiative effect [15,19,20], the fast

* Corresponding author.
E-mail address: huangping@mail.iap.ac.cn (P. Huang).

https://doi.org/10.1016/j.scib.2022.07.010
2095-9273/

ocean response to CO_2 during the first 10 years and the subsequent slow response [21–23]. Moreover, these multi-timescale processes could be tangled up during a combined ramp-up/ramp-down scenario, forming a complex time-evolving pattern of tropical rainfall changes [19,21,24–26].

Here, we use two idealized CO_2 experiments—namely, 1pctCO2 from phase 6 of the Coupled Model Intercomparison Project (CMIP6) [27,28] and 1pctCO2-cdr from the Carbon Dioxide Removal Model Intercomparison Project (CDRMIP) [24]—to represent CO_2 ramp-up and ramp-down, respectively. By combining years 1–139 in 1pctCO2 and years 1–140 in 1pctCO2-cdr, we can obtain a CO_2 ramp-up/ramp-down scenario of CO_2 emissions (green curve in Fig. 1a). The CO_2 continuously increases at 1% a^{-1} from the pre-industrial level to a quadrupled level during the ramp-up period, followed by a ramp-down at the same rate of 1% a^{-1} to reach the pre-industrial level where it is maintained for the final 60 years. The climatology of the first 100 years in the piControl experiment of CMIP6 defines the reference. A detailed description of the experiments is provided next, in Section 2.

2. Materials and methods

2.1. CMIP6

We use four experiments from six CMIP6 models (https://esgf-node.llnl.gov/projects/esgf-llnl/) [27] in this study: piControl, abrupt-4xCO2, 1pctCO2 and 1pctCO2-cdr [24]. The details of these experiments are provided in Table 1. The 1pctCO2 experiment is 150 years long; however, the CO_2 concentration reaches four times that of piControl after 139 years. In the 1pctCO2-cdr experiment, after 140 years of CO_2 removal, a pre-industrial CO_2 level must be held for at least 60 years. We combine years 1–139 in 1pctCO2 and 1–140 in 1pctCO2-cdr to obtain a CO_2 ramp-up/ramp-down scenario of CO_2 emissions. Therefore, across the whole CO_2 ramp-up/ramp-down experiment, the CO_2 ramp-up period is years 1–139, the ramp-down period is years 140–279, and thereafter the stabilization period at the pre-industrial CO_2 level is years 280–339. In terms of model selection, those models that participate in these experiments and provide the variables needed in this study are chosen, which are: ACCESS-ESM1-5, CanESM5, CESM2,

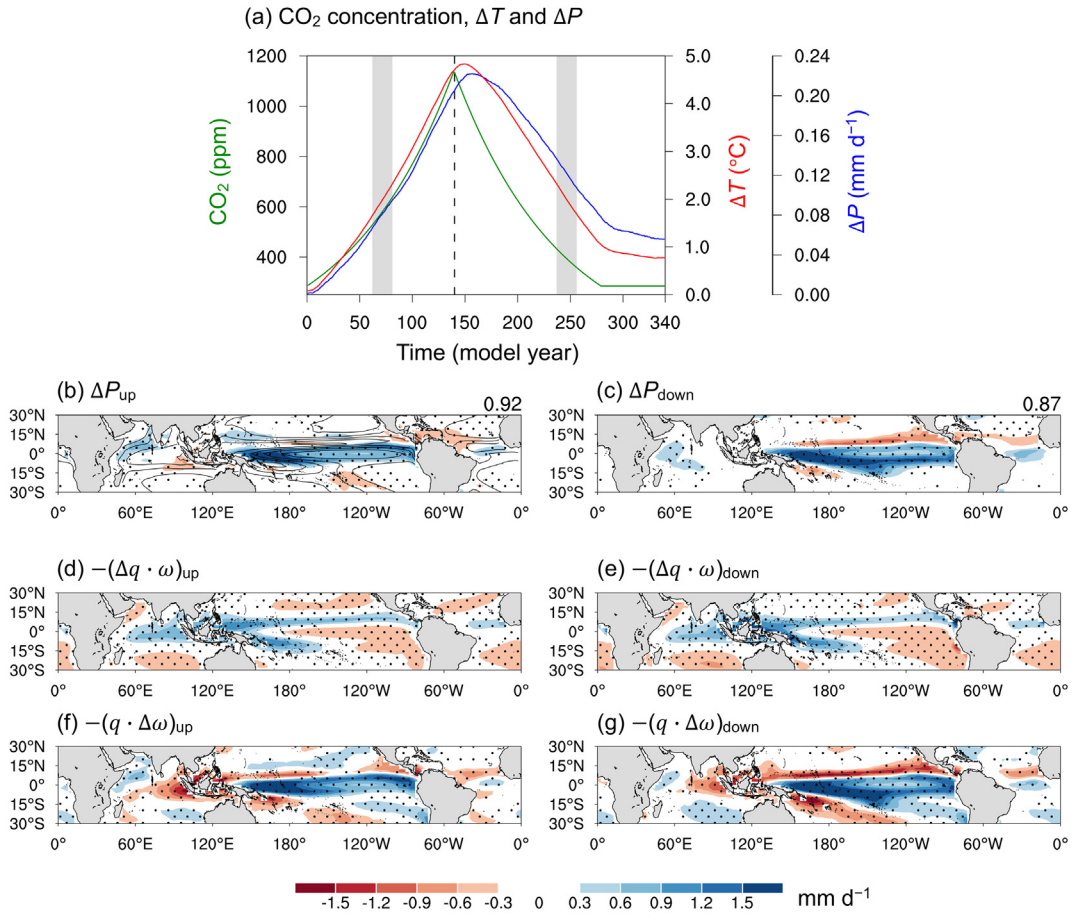

审图号: GS 京(2022)0239 号

Fig. 1. Evolution of global mean and patterns of change in surface temperature and rainfall during the CO_2 ramp-up and ramp-down periods. (a) The 21-year running mean of atmospheric CO_2 concentration (green) and the annual-mean changes in global mean surface temperature (red) and rainfall (blue) in the CO_2 ramp-up/ramp-down experiment. The dashed vertical line indicates year 140, when the CO_2 concentration peaks. The two grey bands covering years 62–81 and 237–256 denote the two representative time slices of 2 °C global mean warming during ramp-up and ramp-down. Changes in tropical rainfall (b, c) and the thermodynamic (d, e) and dynamic (f, g) components in the 2 °C warming time slices during CO_2 ramp-up (b, d, f) and ramp-down (c, e, g). The contours in (b) represent the climatology of tropical rainfall in piControl (interval: 2 mm d^{-1}). The spatial correlation coefficients between the sum of the thermodynamic and dynamic components and tropical rainfall changes are shown in the top-right corners of (b) and (c). Stippling in (b–g) indicates that at least five out of six models agree on the sign of the multi-model mean.

Table 1
Experiments used in this study.

Experiment name	Experiment design	Time
piControl	Pre-industrial control simulation (the global mean atmospheric CO_2 concentration of 284.7 ppm)	At least 500 years
abrupt-4xCO2	Forced by an abruptly quadrupling of the pre-industrial CO_2 level (1138.8 ppm), which is then held constant for 150 years	150 years
1pctCO2	Forced by CO_2 increased at a rate of 1% a^{-1} from the pre-industrial CO_2 level	150 years
1pctCO2-cdr	Forced by CO_2 decreased at a rate of 1% a^{-1} from the quadrupled to pre-industrial CO_2 level, which is then held constant for 60 years	At least 200 years

CNRM-ESM2-1, GFDL-ESM4, and MIROC-ES2L. We perform the sign agreement test to examine whether or not the regional climate change is robust in individual models.

2.2. Fast and slow decomposition of the climate response

The regional climate response to CO_2 forcing is contributed to the processes at different timescales. Specifically, there are three main components related to different timescales—rapid adjustment, and fast and slow SST-driven responses [21,22]. The first of these, i.e., rapid adjustment, is the direct response of the climate to CO_2 forcing on short timescales of weeks to months, while the latter two, i.e., the fast and slow SST-driven responses, are the responses induced by the short- and long-term SST responses, respectively. Previous studies [21,22] have proposed a timescale decomposition method to elucidate the processes at different timescales, based on the linear assumption that the climate response under any CO_2 forcing scenario can be reconstructed by the sum of responses at different timescales to abrupt CO_2 forcing [29]. The abrupt CO_2 forcing in the abrupt-4xCO2 experiment induces rapid warming before year 10, after which the rate of global warming decreases to below 0.1 °C a^{-1} (Fig. S1a online). A similar evolution can be found in the response of tropical-mean rainfall (Fig. S1b online).

Following this method in the literatures [21,22], the rapid adjustment and fast SST-driven response are considered together as a total fast response, while the slow SST-driven response is considered as the slow response. The fast response is defined as the difference between the climatology of years 1–10 (initiated from year 1) in the abrupt-4xCO2 experiment and the pre-industrial climatology of the first 100 years in the piControl experiment. The slow response is defined as the difference between the climatology of years 131–150 and that of years 1–10 in the abrupt-4xCO2 experiment. Although the climatology calculated from the 10-year datasets (from year 1 to year 10) could include the signal of internal variability, the global warming trend dominates the SST changes in the central and eastern equatorial Pacific (5°S–5°N, 160°–80°W) in the abrupt-4xCO2 experiment, as shown in Fig. S2 (online).

In the CO_2 ramp-up/ramp-down experiment, the contributions of the fast and slow responses to global warming are calculated based on their spatial patterns of global surface warming (Fig. S3 online). For any given year, the annual-mean surface warming pattern can be regressed onto the surface warming pattern of the fast and slow responses normalized by their corresponding global mean surface temperature. In the spatial regression, the two-dimensional array of the surface warming pattern is first reshaped into a one-dimensional array. This multiple linear regression can be expressed as

$$\Delta T_{\mathrm{up/down}}(t) = F(t)\cdot\frac{\Delta T_{\mathrm{fast}}}{\overline{\Delta T}_{\mathrm{fast}}} + S(t)\cdot\frac{\Delta T_{\mathrm{slow}}}{\overline{\Delta T}_{\mathrm{slow}}} + r(t), \tag{1}$$

where $\Delta T_{\mathrm{up/down}}(t)$ is the surface warming pattern in the CO_2 ramp-up/ramp-down simulation; ΔT_{fast} and ΔT_{slow} are the surface warming patterns of the fast and slow responses, respectively; Δ represents change under CO_2 forcing; and the overbar indicates the global mean. As the regression coefficients, $F(t)$ and $S(t)$ define the time-varying contributions of responses at different timescales to the warming during CO_2 ramp-up/ramp-down. As a residual component, $r(t)$ is linearly independent from the fast and slow responses. The reconstruction of the global mean ΔT (magenta curve in Fig. 2g) by the ΔT_{fast} and ΔT_{slow} resembles the evolution of directly projected global mean ΔT (black curve in Fig. 2g). All the analyses for Eq. (1) are performed based on the annual-mean and multi-model ensemble mean.

2.3. Reconstruction of the time-dependent response

The $F(t)$ and $S(t)$ coefficients are further used to reconstruct the fast and slow responses of other variables [21,22], such as the precipitation or circulation, in the CO_2 ramp-up/ramp-down experiment. The reconstructed fast and slow responses of variable Y along with the evolution of the CO_2 ramp-up/ramp-down scenario ($\Delta Y_{\mathrm{CDR\_fast}}(t)$ and $\Delta Y_{\mathrm{CDR\_slow}}(t)$) can be expressed as

$$\Delta Y_{\mathrm{CDR\_fast}}(t) = F(t)\cdot\frac{\Delta Y_{\mathrm{fast}}}{\overline{\Delta T}_{\mathrm{fast}}}, \tag{2}$$

and

$$\Delta Y_{\mathrm{CDR\_slow}}(t) = S(t)\cdot\frac{\Delta Y_{\mathrm{slow}}}{\overline{\Delta T}_{\mathrm{slow}}}, \tag{3}$$

where ΔY_{fast} and ΔY_{slow} are the corresponding fast and slow responses, respectively.

2.4. Surface energy budget analyses

The formation of the changes in the SST pattern can be evaluated based on the ocean surface energy budget balance [6]. In the ocean mixed layer, it can be written as

$$\Delta Q_t = \Delta D_{\mathrm{o}} + \Delta Q_{\mathrm{net}}, \tag{4}$$

where $Q_t = \rho_{\mathrm{o}} C_{\mathrm{p}} h \partial T/\partial t$ is the heat storage of the mixed layer, in which ρ_{o} and C_{p} are the density and specific heat of seawater, h is the depth of the mixed layer and T is the SST; D_{o} is the ocean heat transport convergence; and $Q_{\mathrm{net}} = Q_{\mathrm{S}} + Q_{\mathrm{L}} + Q_{\mathrm{H}} + Q_{\mathrm{E}}$ is the net surface heat flux (or the ocean heat uptake), in which Q_{S} is the net surface shortwave radiation flux, Q_{L} is the net surface longwave radiation flux, and Q_{H} and Q_{E} are the surface sensible and latent heat flux, respectively. Positive flux denotes warming of the ocean. Here, the h in the tropical ocean is chosen as a constant of 50 m for simplicity, as in a previous study [30]. Due to the varying mixed-layer depth outside the tropics, the global pattern of ocean surface energy budget is just for rough reference. The oceanic dynamics D_{o} can be diagnosed by the surface energy budget balance, i.e., Eq. (4).

Moreover, D_{o} can be further decomposed into changes in the ocean three-dimensional advection, as follows:

$$\begin{aligned}\Delta D_{\mathrm{o}} = -\rho_{\mathrm{o}} C_{\mathrm{p}} \Bigg[&\int_{-h}^{0} \Delta u \frac{\partial T}{\partial x}\mathrm{d}z + \int_{-h}^{0} u \frac{\partial \Delta T}{\partial x}\mathrm{d}z + \int_{-h}^{0} \Delta v \frac{\partial T}{\partial y}\mathrm{d}z \\ &+ \int_{-h}^{0} v \frac{\partial \Delta T}{\partial y}\mathrm{d}z + \int_{-h}^{0} \Delta w \frac{\partial T}{\partial z}\mathrm{d}z + \int_{-h}^{0} w \frac{\partial \Delta T}{\partial z}\mathrm{d}z \Bigg] + \Delta R,\end{aligned} \tag{5}$$

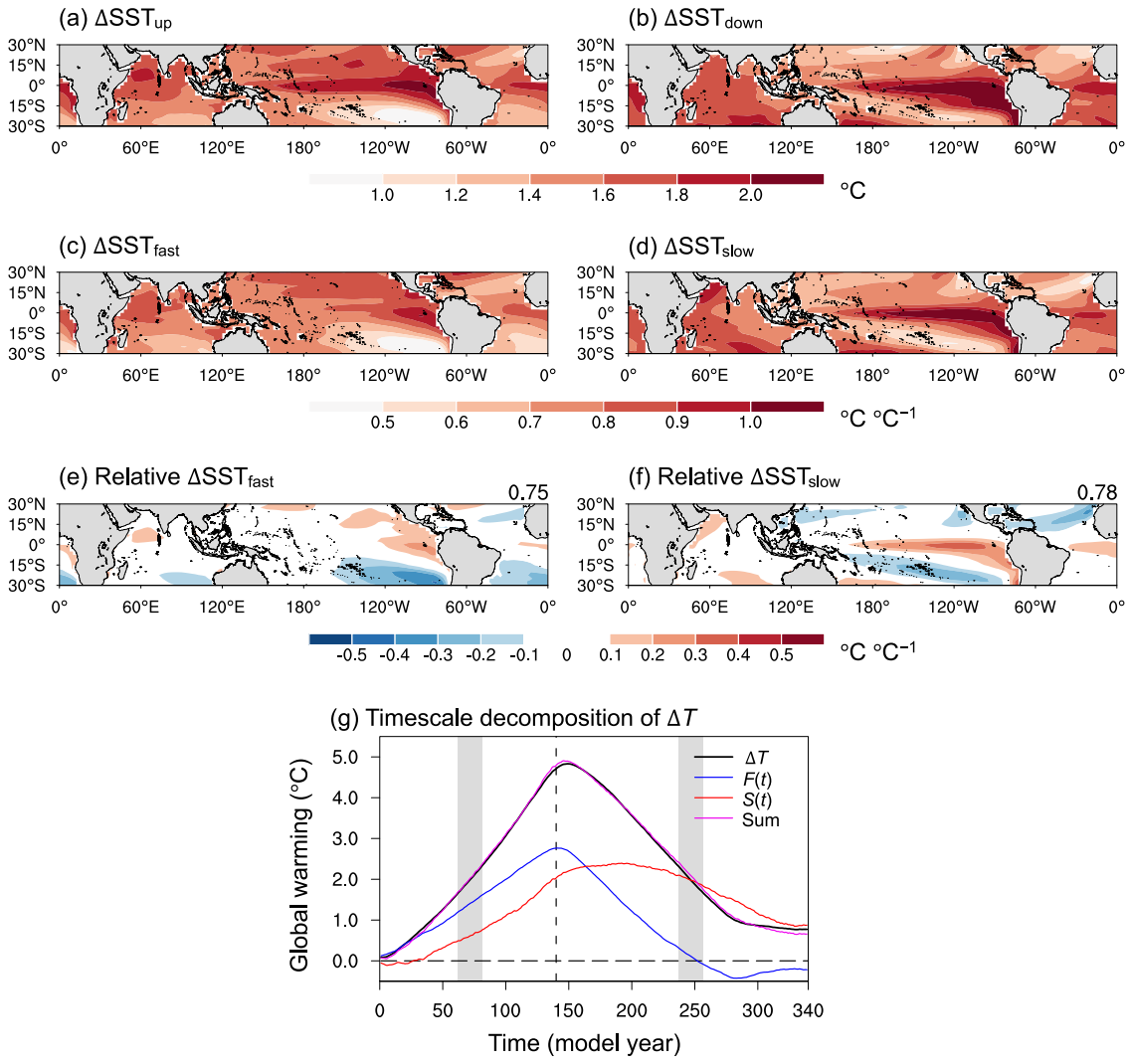

Fig. 2. Pattern of tropical SST changes and the timescale decomposition. Changes in tropical SST in 2 °C warming time slices during CO_2 ramp-up (a) and -down (b). The normalized fast (c) and slow (d) changes in tropical SST. (e, f) As in (c, d) but with the tropical mean (shown in the top-right corner) removed. (g) The 21-year running mean contribution of the fast ($F(t)$; blue) and slow ($S(t)$; red) responses in the CO_2 ramp-up/ramp-down experiment. Their sum (purple) is shown to compare with the total global mean warming (black). The dashed vertical line and two grey bands are the same as in Fig. 1a.

where T represents the ocean temperature, u, v, and w are the zonal, meridional and vertical ocean current, respectively; and ΔR is the residual term, including the changes in heat transport related to certain subgrid-scale processes [31]. For simplicity, we rewrite Eq. (5) as

$$\Delta D_o = D_{\Delta u\_T} + D_{u\_\Delta T} + D_{\Delta v\_T} + D_{v\_\Delta T} + D_{\Delta w\_T} + D_{w\_\Delta T} + \Delta R, \qquad (6)$$

in which $D_{\Delta u\_T}$, $D_{\Delta v\_T}$, and $D_{\Delta w\_T}$ denote the changes in heat transport due to changes in ocean currents, and $D_{u\_\Delta T}$, $D_{v\_\Delta T}$, and $D_{w\_\Delta T}$ denote the changes in heat transport due to changes in temperature gradients. Limited by the ocean variables provided by the CDRMIP models, we only perform the analysis related to Eqs. (5) and (6) on the fast and slow responses based on the piControl and abrupt-4xCO2 experiments in five out of the six models, i.e., all models except GFDL-ESM4.

3. Results

3.1. Asymmetric change in tropical rainfall between the CO_2 ramp-up and ramp-down

During the CO_2 ramp-up and ramp-down periods, the changes in global mean surface temperature (ΔT; red curve in Fig. 1a) and rainfall (ΔP; blue curve in Fig. 1a) are obviously asymmetric and lag the CO_2 concentration, agreeing with previous studies [15,16]. Two 20-year slices (years 62–81 and 237–256; gray bands in Fig. 1a), representative of when the global mean surface warming increases to 2 °C during CO_2 ramp-up and returns to 2 °C during CO_2 ramp-down, are chosen to exclude the influence of the well-known delay in global mean surface warming during CO_2 ramp-down (Fig. 1a) [15,16]. The tropical rainfall changes during CO_2 ramp-up (ΔP_{up}; Fig. 1b) mainly show a hook-like increase pattern over the equatorial Pacific, consistent with the result in the

RCP4.5 experiment of CMIP5 models [32]. The rainfall changes during CO_2 ramp-down (ΔP_{down}; Fig. 1c) are much stronger than ΔP_{up}, with stronger spatial variation. The root-mean-square of ΔP_{down} in Fig. 1c is around 25% larger than that of ΔP_{up} in Fig. 1b. Differing to ΔP_{up}, the positive changes in ΔP_{down} over the equatorial Pacific extend southwards along the equatorward flank of the South Pacific convergence zone (SPCZ), and there are apparent negative changes over the Pacific intertropical convergence zone (ITCZ) and SPCZ (Fig. S4 online). The pattern of ΔP_{down}, i.e., a southward-shifting Pacific ITCZ and a northward-shifting SPCZ, suggests a stronger narrowing of the tropical rainfall band than that of ΔP_{up} [10,33]. The results in Fig. 1 are analyzed based on two selected parameters—the 20-year periods and the 2 °C global mean warming. We also carry out the analysis on the basis of 30- and 40-year time slices with 2 °C warming (Figs. S5 and S6 online), and with 1 and 3 °C warming (Figs. S7 and S8 online). All the results are closely consistent with those in Fig. 1, indicating the conclusions are independent of the parameters.

Based on the moisture budget, ΔP can be decomposed into the thermodynamic and dynamic components related to the moisture and circulation changes, respectively: $\Delta P \approx -\frac{1}{\rho g}(\Delta q \cdot \omega + q \cdot \Delta\omega)$ [5,10,34], where q is the surface specific humidity, ω is the 500-hPa vertical velocity, ρ is the density of water and g denotes gravitational acceleration. The constants are omitted for conciseness hereafter. The patterns of the sum of $\Delta q \cdot \omega$ and $q \cdot \Delta\omega$ (Fig. S9 online) closely resemble those of ΔP_{up} and ΔP_{down}, respectively.

The thermodynamic component ($-\Delta q \cdot \omega$; Fig. 1d, e) shows increased precipitation over the rising branches of background tropical circulation, reflecting the wet-get-wetter mechanism [4,5]. In the two representative time slices of 2 °C global mean warming, $-(\Delta q \cdot \omega)_{up}$ and $-(\Delta q \cdot \omega)_{down}$ are almost the same (Fig. 1d, e). As a result, the different ΔP between CO_2 ramp-up and ramp-down is dominated by the dynamic components ($-(q \cdot \Delta\omega)_{up}$ and $-(q \cdot \Delta\omega)_{down}$; Fig. 1f, g). The $-(q \cdot \Delta\omega)_{up}$ mainly shows a zonal dipole structure between the tropical Pacific and Indian oceans, whereas $-(q \cdot \Delta\omega)_{down}$ is characterized by negative changes over the climatological rain band and positive changes over the equatorial Pacific with some southward extension. The magnitudes of ΔP_{up} and ΔP_{down} are much weaker over the tropical Indian Ocean than over the tropical Pacific owing to the counteraction between $-\Delta q \cdot \omega$ and $-q \cdot \Delta\omega$.

The dynamic component mainly reflects the warmer-get-wetter mechanism, dominated by the SST warming pattern [6,7,14,35]. Fig. 2a, b shows the SST changes in the 2 °C warming time slices during CO_2 ramp-up (ΔSST_{up}) and ramp-down (ΔSST_{down}). An El Niño-like warming pattern [36] emerges during ramp-up (Fig. 2a), but it is much stronger during ramp-down, and with wider meridional extension (Fig. 2b). This El Niño-like warming pattern shows little seasonal variation (figure not shown), leading to an almost constant effect on the equatorial Pacific. Moreover, the SST increase is stronger over the northern than the southern hemisphere during CO_2 ramp-up, consistent with previous results under scenarios of monotonic CO_2 increase [19,37], whereas the inter-hemispheric difference in ΔSST_{up} almost disappears during ramp-down (Fig. 2b). As a result, the ΔSST_{down} in the tropics is dominated by the El Niño-like warming pattern with a stronger meridional gradient and a wider southward extension in the tropical Pacific.

3.2. Fast and slow responses of tropical SST change

The time-dependent SST responses during the two periods are a hybrid of responses at different timescales [15,19,26,38,39]. Fig. 2c, d shows the normalized fast and slow responses of the tropical SST (ΔSST_{fast} and ΔSST_{slow}), respectively. The ΔSST_{fast} exhibits an apparent inter-hemispheric difference (Fig. 2c) like that of the ΔSST_{up} in Fig. 2a, which is weak in ΔSST_{slow}. The almost absent inter-hemispheric difference in ΔSST_{slow} could be related to the reverse changes in ocean heat uptake of the Southern Ocean in the slow response relative to the fast response [15,16,40–42]. On the other hand, the main feature of ΔSST_{slow} is the El Niño-like warming pattern over the eastern equatorial Pacific, with a much stronger amplitude and wider southward extension than ΔSST_{up} [22]. The distinctions between the patterns of ΔSST_{fast} and ΔSST_{slow} can be observed more clearly in the relative SST changes (Fig. 2e, f), defined as the deviation from the tropical mean [6,10]. The spatial gradient of the relative ΔSST_{slow}, especially in the tropical Pacific, is much larger than that of the relative ΔSST_{fast}, implying stronger impacts of ΔSST_{slow} than ΔSST_{fast} under the same global mean warming [43].

The formation of distinct patterns of the fast and slow SST changes can be investigated from the decomposition of the surface energy budget (Fig. S10 online). For the SST changes in the mid-to-high latitudes, the inter-hemispheric difference in ΔSST_{up} can be clearly understood from the reverse ΔD_o of the Southern Ocean (Fig. S10k, l online) leading to reverse changes in the ocean heat uptake of the Southern Ocean. In the fast response, there is surface warming (Fig. S3a online) and negative ΔD_o (Fig. S10k online) along the southern flank of the Antarctic Circumpolar Current (45°–60°S), denoting additional heat is absorbed by the ocean. In the slow response, the positive ΔD_o of the Antarctic Circumpolar Current (Fig. S10l online) and equatorial Pacific, reflecting that the ocean loses heat to the atmosphere, explains the weak inter-hemispheric difference and strong El Niño-like warming pattern in ΔSST_{slow}, respectively.

To reveal the regional processes responsible for forming the stronger El Niño-like warming pattern in ΔSST_{slow} than in ΔSST_{fast}, we decompose the tropical ΔD_o into the changes in heat transport due to changes in ocean currents ($D_{\Delta u\_T}$, $D_{\Delta v\_T}$, and $D_{\Delta w\_T}$) and temperature gradients ($D_{u\_\Delta T}$, $D_{v\_\Delta T}$, and $D_{w\_\Delta T}$). The sum of all decomposed components (Fig. S10 online) accords well with the ΔD_o calculated as the residual of the sea surface energy budget balance (Eq. (4)). Among all the components (Fig. S11 online), terms $D_{\Delta u\_T}$, $D_{\Delta w\_T}$, and $D_{w\_\Delta T}$ contribute most to the formation of the stronger El Niño-like warming pattern in ΔSST_{slow} (Fig. 3). The two terms $D_{\Delta u\_T}$ (Fig. 3c, d) and $D_{\Delta w\_T}$ (Fig. 3e, f) are associated with the slowdown of oceanic circulation (Fig. 3i, j) and Walker circulation under global warming [44,45]. However, the stronger slowdown in circulation could be coupled with the stronger El Niño-like warming pattern due to the Bjerknes feedback, suggesting an amplifying effect on, but not the cause of, the SST warming pattern.

The negative $D_{w\_\Delta T}$ reflects the ocean dynamical thermostat (ODT) mechanism [23,46,47], which is induced by faster surface warming under the CO_2 radiative forcing. The negative $D_{w\_\Delta T}$ with the ODT mechanism favors a La Niña-like warming pattern, contributing negatively to the overall El Niño-like warming pattern [47,48]. In the fast response, the surface warming is much larger than the subsurface (below 100 m) warming (Fig. 3i), inducing a strong ODT effect (Fig. 3g); whereas in the slow response, the subsurface warming is more enhanced (Fig. 3j), suggesting a more suppressed ODT effect (Fig. 3h). As a result, the more suppressed negative effect of the ODT mechanism in the slow response leads to a stronger overall oceanic dynamic effect (ΔD_o, Fig. 3a, b), and thus a stronger El Niño-like warming pattern, in ΔSST_{slow}, similar to the findings of a previous study [49].

3.3. Varying contributions of fast and slow responses

The contribution of the fast response ($F(t)$; blue curve in Fig. 2g) increases linearly during CO_2 ramp-up, as revealed in previous studies [21,22], and then falls during CO_2 ramp-down, largely fol-

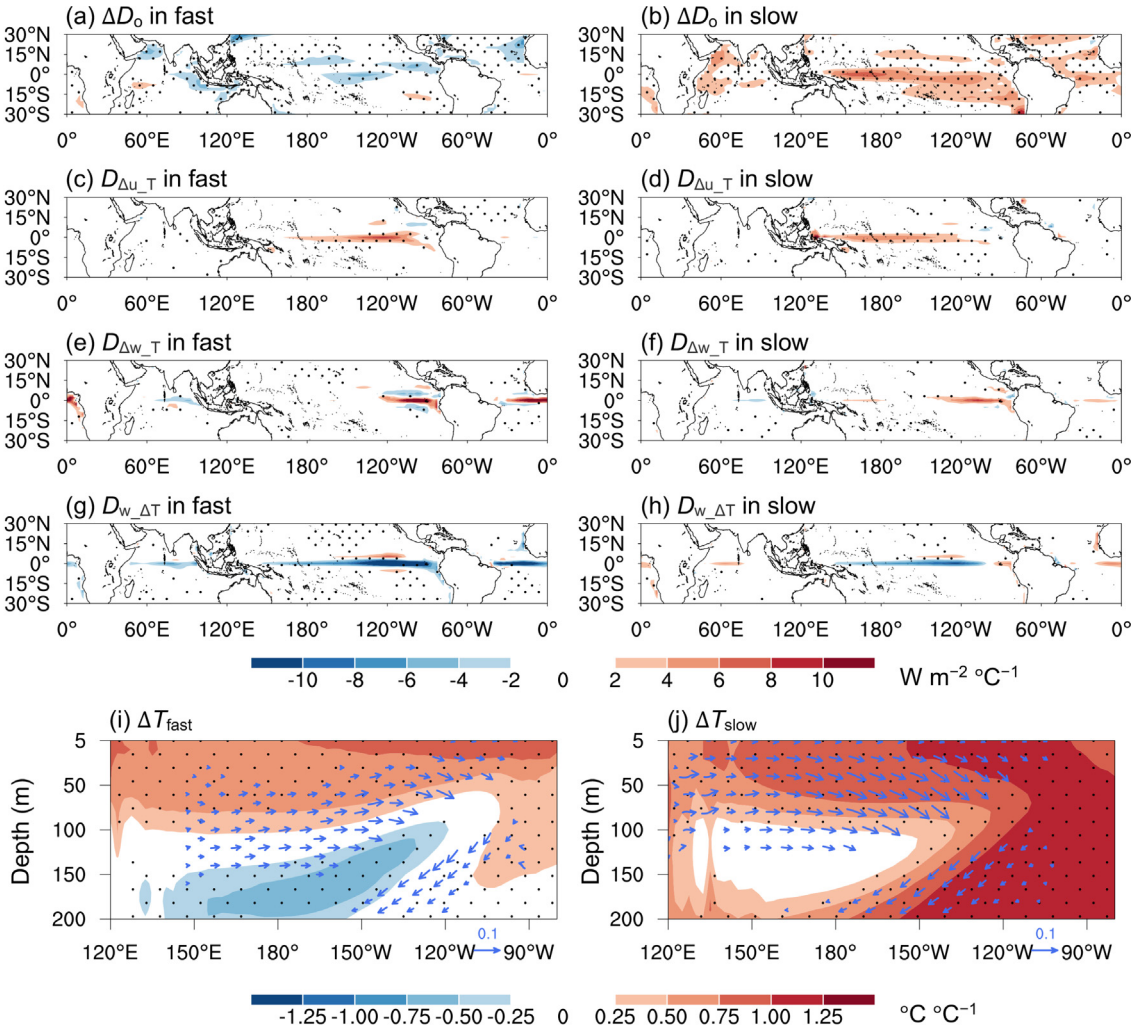

审图号: GS 京(2022)0239 号

Fig. 3. Fast and slow changes in ocean heat transport in the mixed layer during CO_2 ramp-up and ramp-down. The normalized fast (a) and slow (b) changes in ocean heat transport calculated by the diagnostic relationship in Eq. (4). (c, d) As in (a, b) but for the ocean zonal heat transports due to the changes in ocean zonal currents. (e, f) As in (a, b) but for the ocean vertical heat transports due to the changes in ocean vertical currents. (g, h) As in (a, b) but for the ocean vertical heat transport due to the changes in ocean temperature. (i, j) As in (a, b) but for the changes in equatorial-mean (2.5°S–2.5°N) ocean temperature (shaded) and currents (vectors) in the Pacific. The vertical velocity is multiplied by 10^3 for display purposes, and vectors that do not pass the sign agreement test are omitted. Stippling indicates that at least five out of six models agree on the sign of the multi-model mean.

lowing the time evolution of the CO_2 concentration (green curve in Fig. 1a) with a small delay of 10 years. In contrast, the contribution of the slow response ($S(t)$; red curve in Fig. 2g) is not pronounced during the first 40 years [21,22] and gradually increases until 60 years after the CO_2 starting to ramp down, lagging the peak CO_2 concentration remarkably. After the CO_2 concentration restores to the pre-industrial CO_2 level (year 279), the slow response dominates the total climate response. The linear combination of the asynchronous fast and slow responses can depict the time-varying response during CO_2 ramp-up and ramp-down well.

The tropical circulation is the key bridge across which the pattern of SST change influences the dynamic component of rainfall changes in the warmer-get-wetter mechanism [6]. The fast circulation changes ($\Delta\omega_{fast}$; Fig. 4a) differ notably from the slow circulation changes ($\Delta\omega_{slow}$; Fig. 4b), both in pattern and amplitude. The $\Delta\omega_{fast}$ presents a near dipole pattern over the tropical Pacific–Indian Ocean (Fig. 4a). The $\Delta\omega_{slow}$, much stronger than $\Delta\omega_{fast}$, exhibits upward changes over the equatorial Pacific and its southern flank and downward changes over the climatological rain band (Fig. 4b). The $\Delta\omega_{fast}$ and $\Delta\omega_{slow}$ dominate the patterns of the dynamic components of the fast $(-(q\cdot\Delta\omega)_{fast}$; Fig. 4c) and slow $(-(q\cdot\Delta\omega)_{slow}$; Fig. 4d) responses, respectively, due to the weak spatial gradient of background moisture. The discrepancies between $-(q\cdot\Delta\omega)_{fast}$ and $-(q\cdot\Delta\omega)_{slow}$ correspond to those between ΔSST_{fast} and ΔSST_{slow}, following the warmer-get-wetter mechanism. From a zonal-mean perspective, the southward shift of the ITCZ in the northern hemisphere and the wider southward extension of upward changes over the equatorial Pacific in $-(q\cdot\Delta\omega)_{slow}$ could induce a southward shift of the tropical rainfall band, implying a role played by the inter-hemispheric difference in global SST changes (Fig. S3 online) due to the global energy balance [18,50]. Regionally, however, the northward shift of the SPCZ in $-(q\cdot\Delta\omega)_{slow}$ is contrary to the southward shift of the zonal-mean rain band, highlighting the role of the tropical pattern of ΔSST_{slow} [14].

Regarding the thermodynamic component, although the pattern of fast moisture changes (Δq_{fast}; Fig. S12a online) differs from that of the slow moisture changes (Δq_{slow}; Fig. S12b online), the

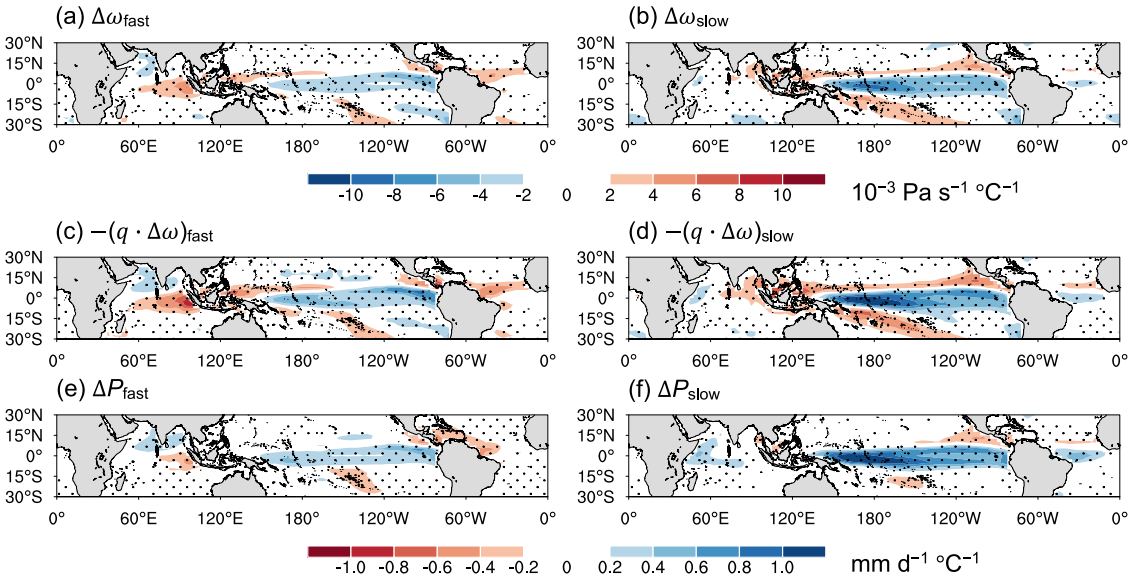

Fig. 4. Patterns of fast and slow changes in tropical rainfall, circulation and the dynamic components. The normalized fast (a) and slow (b) changes in 500-hPa vertical pressure velocity. (c, d) As in (a, b) but for the dynamic component of tropical rainfall changes. (e, f) As in (a, b) but for the tropical rainfall changes. Stippling indicates that at least five out of six models agree on the sign of the multi-model mean.

weak spatial gradients in moisture changes cannot induce apparent differences in the thermodynamic components of the fast and slow responses (Fig. S12c, d online), which both show a wet-get-wetter pattern at the climatological rain band. The thermodynamic components can offset the decreases in the dynamic components at the climatological rain band, resulting in the fast and slow rainfall changes (Fig. 4e, f), basically following a warmer-get-wetter pattern [6]. In addition, ΔP_{slow} shows stronger positive changes than ΔP_{fast} in the equatorial Pacific and apparent negative changes in the Pacific ITCZ and SPCZ (Fig. 3e, f), as in the dynamic components (Fig. 3c, d) and the circulation changes (Fig. 3a, b) driven by ΔSST_{slow}. The stronger increase of ΔP_{slow} than ΔP_{fast} in the equatorial Pacific indicates a stronger narrowing of the ITCZ in the slow response corresponding to the pattern of ΔSST_{slow} with a stronger El Niño-like pattern. For the Indian Ocean, the horizontal gradients of ΔSST_{fast} and ΔSST_{slow} (Fig. 2c–f) are weaker relative to those over the Pacific, and the dynamic component basically counteracts the thermodynamic component (Fig. 1d–g). Therefore, the difference between ΔP_{up} and ΔP_{down} is weak in the Indian Ocean, although there are some differences between ΔSST_{fast} and ΔSST_{slow} (Fig. 2).

Based on the mechanisms revealed from the decomposed fast and slow changes in rainfall, circulation and relative SST, it is possible to understand the time evolution of their changes during CO_2 ramp-up/ramp-down. The fast and slow changes during a given period can be reconstructed by the time-varying coefficients ($F(t)$ and $S(t)$) and the spatial patterns (Figs. 2c, d and 4) of the fast and slow responses [21] (see Methods section for further details). As expected with the time-varying coefficients (Fig. 2g), the fast SST changes are much stronger than the slow SST changes during CO_2 ramp-up, and *vice versa* during CO_2 ramp-down (Fig. S13 online). However, the spatial gradient of the relative $\Delta SST_{up\text{-}slow}$ (Fig. 5b) is comparable with that of the relative $\Delta SST_{up\text{-}fast}$ (Fig. 5a), whereas the relative $\Delta SST_{down\text{-}slow}$ (Fig. 5d) overwhelms the relative $\Delta SST_{down\text{-}fast}$ (Fig. 5c). Driven by these relative ΔSST, the respective dynamic components (Fig. 5e–h) basically follow the patterns of the dynamic components in Fig. 4c, d and the amplitudes of these relative ΔSST.

The negative rainfall changes in the dynamic component during CO_2 ramp-up (Fig. 5e, f) over the climatological rain band are offset by the thermodynamic component (figure not shown) [5,7,10,34], leading to only positive rainfall changes in the tropical Pacific ($\Delta P_{up\text{-}fast}$ and $\Delta P_{up\text{-}slow}$; Fig. 5i, j). In contrast, during the CO_2 ramp-down period, the strong negative changes of $-(q \cdot \Delta\omega)_{up\text{-}slow}$ (Fig. 5h) over the Pacific ITCZ and SPCZ cannot be totally offset by the increased rainfall from the thermodynamic component (Fig. 1f). These patterns lead to apparent negative rainfall changes over the Pacific ITCZ and SPCZ during CO_2 ramp-down (Figs. 1c and 5l).

4. Discussion

Our results show that the tropical rainfall change has stronger spatial variations during CO_2 ramp-down than ramp-up, with the difference characterized as positive over the equatorial Pacific with a southward extension, and negative over the Pacific ITCZ and SPCZ. These distinct rainfall patterns can be understood by the time-varying contributions from the fast and slow responses during CO_2 ramp-up/ramp-down. The fast response largely follows the CO_2 concentration, with a small delay of 10 years, but the slow response peaks around 60 years after CO_2 starts to ramp down. The pattern of SST change in the slow response is dominated by an El Niño-like pattern, with a stronger meridional gradient and wider southward extension than that of the fast response, inducing larger rainfall and circulation changes. The larger contribution of the slow response and the larger impacts of slow SST changes during CO_2 ramp-down together form the pattern of tropical rainfall changes. The tropical rainfall change with stronger spatial variation during CO_2 ramp-down is independent of the well-known delay of the global mean temperature response to CO_2 ramp-down. Our study suggests another great concern for the persistent impacts of CO_2 emissions as we strive for a certain goal of global mean temperature increase by removing CO_2 in the immediate future.

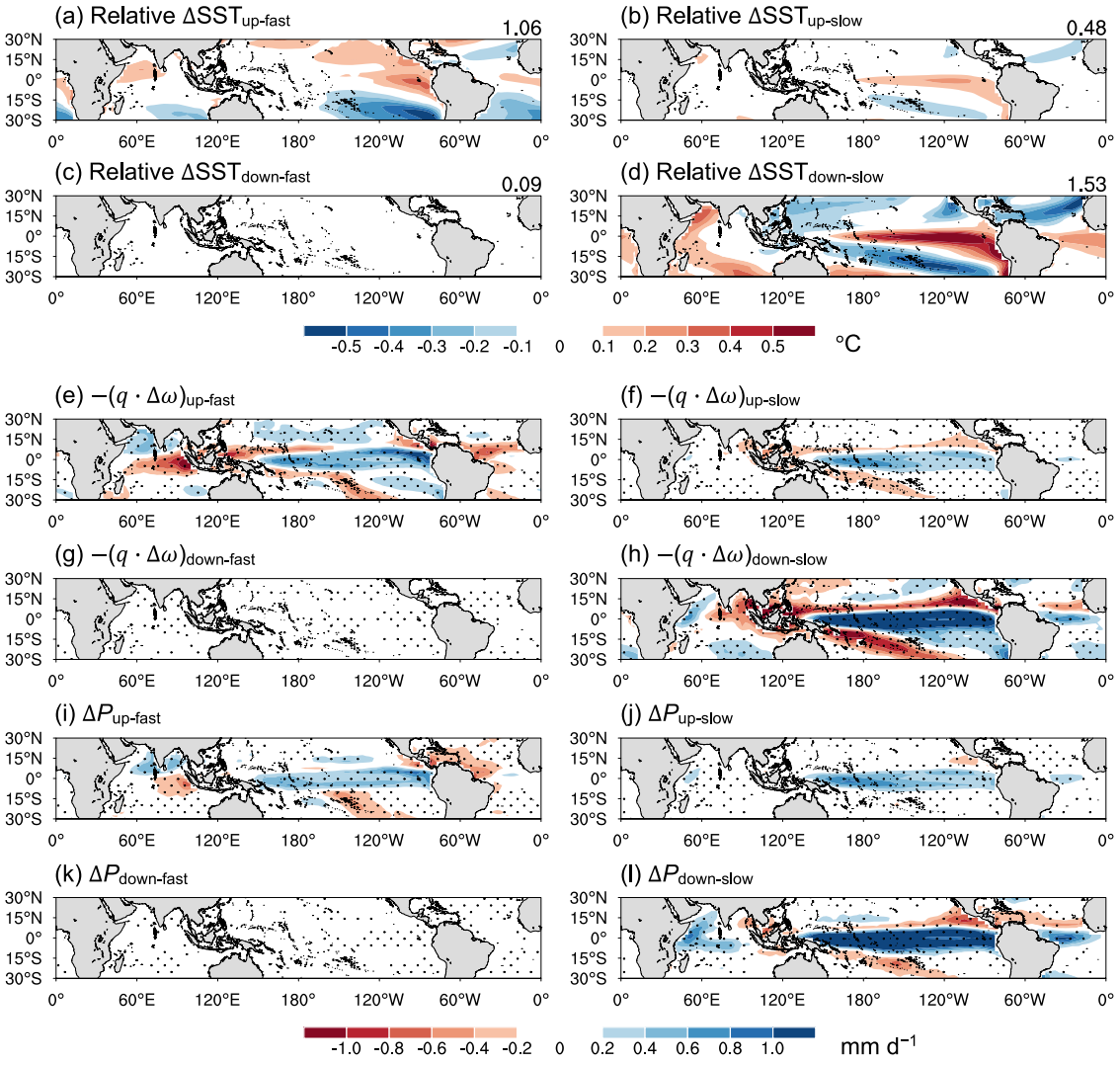

审图号: GS 京(2022)0239 号

Fig. 5. Patterns of the fast and slow changes in relative SST, rainfall, and the dynamic component during CO_2 ramp-up and ramp-down. The fast (a, c) and slow (b, d) changes in tropical SST in 2 °C warming time slices during CO_2 ramp-up (a, b) and ramp-down (c, d), in which the tropical mean (shown in the top-right corner) is removed. (e–h) As in (a–d) but for the dynamic component of tropical rainfall changes. (i–l) As in (a–d) but for the tropical rainfall changes. Stippling in (e–l) indicates that at least five out of six models agree on the sign of the multi-model mean.

The analyses in this study are mainly based on the six CMIP6 models participating in CDRMIP/CMIP6, which are the only available simulations we can access at present. Due to the limited number of models, the multi-model mean result shown here may be model-dependent [51,52]. In particular, the present models suggested a robust El Niño-like warming pattern over the tropical Pacific (one of the dominant factors for tropical climate changes [8,49,53–56]), but the SST warming pattern in the tropical Pacific remains controversial [57,58]. This debatable projection of the SST warming pattern will almost certainly influence the robustness of the changes in tropical rainfall under a CO_2 removal scenario. Such uncertainty due to model limitations might also influence the seasonality of tropical climate change [10,59], even though the present analyses show that the seasonality of the SST warming pattern is weak relative to the annual mean. Thus, more models need to participate in CDRMIP so that we can study the climate response to a CO_2 removal scenario more effectively.

In the present study, the evolution of regional SST is simplified into fast and slow processes. However, the two processes cannot totally depict all the responses of regional SST to CO_2 forcing [21,22]. Fig. S14 (online) validates the applicability of the reconstructed fast and slow responses, and the spatial correlation coefficients of the reconstructions with the directly projected changes are shown in the top-right corners of the panels in the left-hand column of Fig. S14 (online). Although the sum of the reconstructed fast and slow responses captures the main changes, there are some residuals at the southern flank of the equatorial Pacific (Fig. S14d, h, l online) during CO_2 ramp-down, implying that there could, besides the fast and slow processes defined here, be other as yet unclear processes. For the mid-to-high latitudes, the tipping elements in the climate system, such as the Arctic amplification [60] and Atlantic Meridional Overturning Circulation [18], are not linearly dependent on the global mean surface warming [61]. Therefore, the fast–slow timescale decomposition method is limited in terms of capturing the linear responses to global mean surface warming. The residual component should be considered in future work to reveal potential nonlinear processes.

This study mainly focuses on the tropical rainfall over ocean and emphasizes the role of local SST changes, since the majority of the tropics is covered by ocean. However, the changes in rainfall

over land and the associated mechanisms could be different from those over ocean [62–64], which should be studied in the future.

Conflict of interest

The authors declare that they have no conflict of interest.

Acknowledgments

This work was supported by the National Key Research & Development Program of China (2019YFA0606703), the National Natural Science Foundation of China (41975116 and 42105027), the Youth Innovation Promotion Association of the Chinese Academy of Sciences (Y202025), the China Postdoctoral Science Foundation (BX20200329 and 2020M680646), and the Special Research Assistant Project of Chinese Academy of Sciences. The authors acknowledge the World Climate Research Programme's Working Group on Coupled Modeling, which is responsible for CMIP6, and the climate modeling groups for producing and making available their model output. The CMIP6 data are available at https://esgf-node.llnl.gov/projects/esgf-llnl/. We thank the ACCESS Coupled Model Team and Dr. Chloe Mackallah (Commonwealth Scientific and Industrial Research Organisation) for providing some dataset that are not in the CMIP data request. We thank Dr. Yongjie Huang (Institute of Atmospheric Physics, Chinese Academy of Sciences) for providing the map database (https://github.com/huangynj/NCL-Chinamap.git).

Author contributions

Shijie Zhou and Ping Huang conceived the study, performed the analyses, and wrote the paper. Shang-Ping Xie contributed to improving the paper. All authors discussed and commented on the paper.

Appendix A. Supplementary materials

Supplementary materials to this article can be found online at https://doi.org/10.1016/j.scib.2022.07.010.

References

[1] Allen MR, Ingram WJ. Constraints on future changes in climate and the hydrologic cycle. Nature 2002;419:224–32.
[2] Held IM. The partitioning of the poleward energy transport between the tropical ocean and atmosphere. J Atmos Sci 2001;58:943–8.
[3] Zheng X-T, Xie S-P, Lü L-H, et al. Intermodel uncertainty in ENSO amplitude change tied to Pacific ocean warming pattern. J Clim 2016;29:7265–79.
[4] Held IM, Soden BJ. Robust responses of the hydrological cycle to global warming. J Clim 2006;19:5686–99.
[5] Chou C, Neelin JD, Chen C-A, et al. Evaluating the "rich-get-richer" mechanism in tropical precipitation change under global warming. J Clim 2009;22:1982–2005.
[6] Xie S-P, Deser C, Vecchi GA, et al. Global warming pattern formation: sea surface temperature and rainfall. J Clim 2010;23:966–86.
[7] Chadwick R, Boutle I, Martin G. Spatial patterns of precipitation change in CMIP5: why the rich do not get richer in the tropics. J Clim 2013;26:3803–22.
[8] Huang P, Xie S-P. Mechanisms of change in ENSO-induced tropical Pacific rainfall variability in a warming climate. Nat Geosci 2015;8:922–6.
[9] Chadwick R, Good P, Andrews T, et al. Surface warming patterns drive tropical rainfall pattern responses to CO_2 forcing on all timescales. Geophys Res Lett 2014;41:610–5.
[10] Huang P, Xie S-P, Hu K, et al. Patterns of the seasonal response of tropical rainfall to global warming. Nat Geosci 2013;6:357–61.
[11] Wang F, Harindintwali JD, Yuan Z, et al. Technologies and perspectives for achieving carbon neutrality. Innovation 2021;2:100180.
[12] Huang G, Xu Z, Qu X, et al. Critical climate issues toward carbon neutrality targets. Fund Res 2022. https://doi.org/10.1016/j.fmre.2022.02.011.
[13] Wu P, Ridley J, Pardaens A, et al. The reversibility of CO_2 induced climate change. Clim Dyn 2015;45:745–54.
[14] Chadwick R, Wu P, Good P, et al. Asymmetries in tropical rainfall and circulation patterns in idealised CO_2 removal experiments. Clim Dyn 2013;40:295–316.
[15] Cao L, Bala G, Caldeira K. Why is there a short-term increase in global precipitation in response to diminished CO_2 forcing? Geophys Res Lett 2011;38:L06703.
[16] Wu P, Wood R, Ridley J, et al. Temporary acceleration of the hydrological cycle in response to a CO_2 rampdown. Geophys Res Lett 2010;37:L12705.
[17] Song S-Y, Yeh S-W, An S-I, et al. Asymmetrical response of summer rainfall in East Asia to CO_2 forcing. Sci Bull 2022;67:213–22.
[18] Kug J-S, Oh J-H, An S-I, et al. Hysteresis of the intertropical convergence zone to CO_2 forcing. Nat Clim Chang 2021;12:47–53.
[19] Long S-M, Xie S-P, Zheng X-T, et al. Fast and slow responses to global warming: sea surface temperature and precipitation patterns. J Clim 2014;27:285–99.
[20] Li T, Wang Y, Wang B, et al. Distinctive South and East Asian monsoon circulation responses to global warming. Sci Bull 2022;67:762–70.
[21] Zappa G, Ceppi P, Shepherd TG. Time-evolving sea-surface warming patterns modulate the climate change response of subtropical precipitation over land. Proc Natl Acad Sci USA 2020;117:4539–45.
[22] Ceppi P, Zappa G, Shepherd TG, et al. Fast and slow components of the extratropical atmospheric circulation response to CO_2 forcing. J Clim 2018;31:1091–105.
[23] Luo Y, Lu J, Liu F, et al. The role of ocean dynamical thermostat in delaying the El Niño–like response over the equatorial Pacific to climate warming. J Clim 2017;30:2811–27.
[24] Keller DP, Lenton A, Scott V, et al. The carbon dioxide removal model intercomparison project (CDRMIP): rationale and experimental protocol for CMIP6. Geosci Model Dev 2018;11:1133–60.
[25] Manabe S, Bryan K, Spelman MJ. Transient response of a global ocean-atmosphere model to a doubling of atmospheric carbon dioxide. J Phys Oceanogr 1990;20:722–49.
[26] Held IM, Winton M, Takahashi K, et al. Probing the fast and slow components of global warming by returning abruptly to preindustrial forcing. J Clim 2010;23:2418–27.
[27] Eyring V, Bony S, Meehl GA, et al. Overview of the coupled model intercomparison project phase 6 (CMIP6) experimental design and organization. Geosci Model Dev 2016;9:1937–58.
[28] Zhou T. New physical science behind climate change: what does IPCC AR6 tell us? Innovation 2021;2:100173.
[29] Good P, Gregory JM, Lowe JA. A step-response simple climate model to reconstruct and interpret AOGCM projections. Geophys Res Lett 2011;38:L01703.
[30] Dwyer JG, Biasutti M, Sobel AH. Projected changes in the seasonal cycle of surface temperature. J Clim 2012;25:6359–74.
[31] DiNezio PN, Clement AC, Vecchi GA, et al. Climate response of the equatorial Pacific to global warming. J Clim 2009;22:4873–92.
[32] Huang P. Regional response of annual-mean tropical rainfall to global warming. Atmos Sci Lett 2014;15:103–9.
[33] Byrne MP, Schneider T. Narrowing of the ITCZ in a warming climate: physical mechanisms. Geophys Res Lett 2016;43:11350–7.
[34] Seager R, Naik N, Vecchi GA. Thermodynamic and dynamic mechanisms for large-scale changes in the hydrological cycle in response to global warming. J Clim 2010;23:4651–68.
[35] Geng Y-F, Xie S-P, Zheng X-T, et al. Seasonal dependency of tropical precipitation change under global warming. J Clim 2020;33:7897–908.
[36] Collins M, The CMG. El Niño- or La Niña-like climate change? Clim Dyn 2005;24:89–104.
[37] Geoffroy O, Saint-Martin D. Pattern decomposition of the transient climate response. Tellus 2014;66:23393.
[38] Bony S, Bellon G, Klocke D, et al. Robust direct effect of carbon dioxide on tropical circulation and regional precipitation. Nat Geosci 2013;6:447–51.
[39] Bala G, Caldeira K, Nemani R. Fast versus slow response in climate change: implications for the global hydrological cycle. Clim Dyn 2010;35:423–34.
[40] Ma X, Liu W, Allen RJ, et al. Dependence of regional ocean heat uptake on anthropogenic warming scenarios. Sci Adv 2020;6:eabc0303.
[41] Frölicher TL, Sarmiento JL, Paynter DJ, et al. Dominance of the Southern Ocean in anthropogenic carbon and heat uptake in CMIP5 models. J Clim 2015;28:862–86.
[42] Hwang Y-T, Xie S-P, Deser C, et al. Connecting tropical climate change with Southern Ocean heat uptake. Geophys Res Lett 2017;44:9449–57.
[43] Duffy ML, O'Gorman PA, Back LE. Importance of laplacian of low-level warming for the response of precipitation to climate change over tropical oceans. J Clim 2020;33:4403–17.
[44] Vecchi GA, Soden BJ. Global warming and the weakening of the tropical circulation. J Clim 2007;20:4316–40.
[45] Vecchi GA, Soden BJ, Wittenberg AT, et al. Weakening of tropical Pacific atmospheric circulation due to anthropogenic forcing. Nature 2006;441:73–6.
[46] Heede UK, Fedorov AV. Eastern equatorial Pacific warming delayed by aerosols and thermostat response to CO_2 increase. Nat Clim Chang 2021;11:696–703.
[47] Clement AC, Seager R, Cane MA, et al. An ocean dynamical thermostat. J Clim 1996;9:2190–6.
[48] Ying J, Huang P, Huang R. Evaluating the formation mechanisms of the equatorial Pacific SST warming pattern in CMIP5 models. Adv Atmos Sci 2016;33:433–41.

[49] Zheng XT, Hui C, Xie SP, et al. Intensification of El Niño rainfall variability over the tropical Pacific in the slow oceanic response to global warming. Geophys Res Lett 2019;46:2253–60.
[50] Friedman AR, Hwang Y-T, Chiang JCH, et al. Interhemispheric temperature asymmetry over the twentieth century and in future projections. J Clim 2013;26:5419–33.
[51] Xie S-P, Deser C, Vecchi GA, et al. Towards predictive understanding of regional climate change. Nat Clim Chang 2015;5:921–30.
[52] Hawkins E, Sutton R. The potential to narrow uncertainty in regional climate predictions. Bull Am Meteorol Soc 2009;90:1095–107.
[53] Cai W, Wang G, Dewitte B, et al. Increased variability of eastern Pacific El Niño under greenhouse warming. Nature 2018;564:201–6.
[54] Wang G, Cai W, Gan B, et al. Continued increase of extreme El Niño frequency long after 1.5 °C warming stabilization. Nat Clim Chang 2017;7:568–72.
[55] Chakraborty A, Singhai P. Asymmetric response of the Indian summer monsoon to positive and negative phases of major tropical climate patterns. Sci Rep 2021;11:22561.
[56] Chakraborty A. Preceding winter La Niña reduces Indian summer monsoon rainfall. Environ Res Lett 2018;13:054030.
[57] Seager R, Cane M, Henderson N, et al. Strengthening tropical Pacific zonal sea surface temperature gradient consistent with rising greenhouse gases. Nat Clim Chang 2019;9:517–22.
[58] Watanabe M, Dufresne J-L, Kosaka Y, et al. Enhanced warming constrained by past trends in equatorial Pacific sea surface temperature gradient. Nat Clim Chang 2020;11:33–7.
[59] Huang P. Seasonal changes in tropical SST and the surface energy budget under global warming projected by CMIP5 models. J Clim 2015;28:6503–15.
[60] Dai A, Luo D, Song M, et al. Arctic amplification is caused by sea-ice loss under increasing CO_2. Nat Commun 2019;10:121.
[61] Lenton TM, Held H, Kriegler E, et al. Tipping elements in the Earth's climate system. Proc Natl Acad Sci USA 2008;105:1786–93.
[62] Byrne MP, O'Gorman PA. The response of precipitation minus evapotranspiration to climate warming: why the "wet-get-wetter, dry-get-drier" scaling does not hold over land. J Clim 2015;28:8078–92.
[63] Lambert FH, Ferraro AJ, Chadwick R. Land–ocean shifts in tropical precipitation linked to surface temperature and humidity change. J Clim 2017;30:4527–45.
[64] Good P, Booth BB, Chadwick R, et al. Large differences in regional precipitation change between a first and second 2 K of global warming. Nat Commun 2016;7:13667.

Shijie Zhou is a postdoctoral researcher of Institute of Atmospheric Physics, Chinese Academy of Sciences. He received his B.S. degree (2015) from Sun Yat-sen University and Ph.D. degree (2020) in atmospheric science from Institute of Atmospheric Physics, Chinese Academy of Sciences. His research interest focuses on climate change related to monsoons and tropical precipitation under global warming.

Ping Huang is a professor at Institute of Atmospheric Physics, Chinese Academy of Sciences. He received his B.S. degree (2004) from University of Science and Technology of China and Ph.D. degree (2009) in atmospheric science from Institute of Atmospheric Physics, Chinese Academy of Sciences. His research interest focuses on the tropical climate change in the timescales from interannual variability to long-term trend.